Journal of Remote Sensing & GIS
ISSN: 2469-4134

Li et al., J Geophys Remote Sens 2012, 1:1
DOI: 10.4172/2169-0049.1000104

Research Article Open Access

Fusion of Hyperspectral and L-Band SAR Data to Estimate Fractional Vegetation Cover in a Coastal California Scrub Community

Shuang Li[1,2], Christopher Potter[1]*, Cyrus Hiatt[3] and John Shupe[3]

[1]NASA Ames Research Centre Mail Stop 242-4, Moffett Field, CA 94035, USA
[2]Henan University, College of Environment and Planning, Kaifeng, Henan 475004, China
[3]California State University Monterey Bay, Seaside, CA, USA

Abstract

A study was carried out to investigate the utility of airborne hyperspectral and satellite L-band Synthetic Aperture Radar (SAR) data for estimating fractional coverages of herbaceous, coastal scrub, and bare ground cover types on the central California coast. Airborne Visible/Infrared Imaging Spectrometer (AVIRIS) imagery collected in September of 2008 and Phased Array L-band SAR (PALSAR) (HH- and HV-polarizations) captured in April and July of 2008 were combined for vegetation cover mapping. Hyperspectral features, computed as AVIRIS indices (NDVI, TCARI/OSAVI, and PRI), and textural information (energy, contrast, homogeneity, and fractal dimension) produced by L-band SAR were fused together to generate a new feature space. We used global Ordinary Least Squares (OLS) linear regression to integrate and decompose the new feature space for fractional vegetation mapping. Ground measurements of fractional cover were collected from plots located within the U.S. Forest Service's Brazil Ranch study site for validation of the OLS model predictions. Significant linear relationships were found between fractional cover mapping from remote sensing and the ground-truth data. The estimation accuracy of fractional coverage mapping from remote sensing in terms of Root Mean Square Error (RMSE) was 17%, 12%, and 10%, for the herbaceous, coastal scrub, and bare ground covers, respectively. Decomposition results showed that textural information from L-band SAR strongly supported herbaceous and coastal scrub fractional mapping, while indices features from AVIRIS significantly improved mapping of herbaceous cover and bare ground.

Keywords: AVIRIS; ALOS-PALSAR; L-band SAR; Fractional coverage; Coastal scrub

Abbreviations: HBV: Herbaceous; CS: Coastal Scrub; BG: Bare Ground

Introduction

Coastal shrub ecosystems in California have a high degree of biological diversity and endemism, and provide critical habitat for a large number of rare, endangered, and threatened animal and plant species [1]. These mixed herbaceous-shrub communities are of interest because they dominate the central and southern coastal regions of California, but have been largely overlooked as a key biomass carbon component. Coastal scrub covers 7% of the region and is the fourth most extensive vegetation class in the state.

Our study focused on fractional vegetation coverage mapping for herbaceous-shrub ecotypes on the Big Sur coast in Monterey County, CA. The regional-scale products of such remote sensing can uniquely support wildlife habitat mapping and biogeochemical cycling studies. Visible and Near-infrared (V/NIR) imagery from airborne and spaceborne remote sensing have been used in previous studied to investigate the herbaceous-shrub ecotype [2,3]. Hyperspectral imagery has been widely used for vegetation cover mapping [4]. There has been increasing interest in using Synthetic Aperture Radar (SAR) data [5-7], and in combining hyperspectral and SAR data for improved vegetation mapping and estimation of vegetation structural variables [8-11].

Previous studies with satellite SAR for observing vegetation coverage have indicated that backscatter intensity is of little use for forest and shrubland detection at C-band (6 cm) and S-band (10 cm) wavelengths [10-12]. Yatabe [12] compared the research applications of SAR at different radar frequencies (C-, S- and L-band) and found that L-band (24 cm wavelength) was the most effective for discriminating forest and shrubland. Hyperspectral imagery provides many attributes complementary to vegetation canopy information from SAR data and can be used to detect vegetation health status based on spectral characteristics [13,14]. Jouan [9] reported on fusion of SAR and hyperspectral imagery to map land cover by using the evidential fusion method. Blaschke [15] extracted information from SAR and hyperspectral data by an object-based approach. Huang [10] fused Air SAR, AVIRIS and Landsat data for fractional cover mapping in Yellowstone National Park.

In this study, we investigated the fusion of hyperspectral imagery and L-band SAR data for fractional coverage mapping of herbaceous-shrub ecotype in central California. L-band SAR data are available from the Phased Array L-band SAR (PALSAR) instrument, which was installed on the Advanced Land Observing Satellite (ALOS). Hyperspectral imagery from the Airborne Visible/Infrared Imaging Spectrometer (AVIRIS) was collected by NASA Jet Propulsion Laboratory (JPL) in 2008. A new feature space was created by combining spectra information from a standard spectral library, vegetation indices from hyperspectral imagery, and textural information from L-band SAR data. Fractional cover products for herbaceous, coastal scrub, and bare ground were produced by decomposing the new feature space.

***Corresponding author:** Christopher Potter, NASA Ames Research Centre Mail Stop 242-4, Moffett Field, CA 94035, USA, Tel: 650-604-6164; Fax: 650-604-4680; E-mail: chris.potter@nasa.gov

Received May 05, 2012; **Accepted** May 25, 2012; **Published** May 30, 2012

Citation: Li S, Potter C, Hiatt C, Shupe J (2012) Fusion of Hyperspectral and L-Band SAR Data to Estimate Fractional Vegetation Cover in a Coastal California Scrub Community. J Geophys Remote Sensing 1:104. doi:10.4172/2169-0049.1000104

Study Site

The primary research site was located at the Brazil Ranch (center coordinates: latitude 36.35° N, longitude 121.88° W) near Big Sur, California (Figure 1). The Brazil Ranch is named after Tony and Margaret Brazil and the pioneer family that worked to establish the land as a farm, ranch, as well as a dairy operation in the early 20th century. Today, the property serves as a primary research site for the U. S. Forest Service to monitor and manage vegetation, wildlife, water quality, and sensitive coastal habitats.

The Big Sur region is characterized by a Mediterranean climate with rounded ridges, steep sides, and narrow canyons. The terrain is rugged and undulating with the steepest elevation gradients on the Pacific U. S. coast, ranging (over just several km inland) from sea-level up to 1570 meters. Rainfall varies from 40 to 150 cm throughout the range, with the most on the higher mountains in the north. The majority of all precipitation falls in the winter (November-March). During the summer, fog and low clouds are frequent along the coast. Mean annual temperature ranges from 10 to 15°C.

Drier, southeast-facing slopes share a relatively equal distribution of coyote bush (*Baccharis pilularis*) and California coffeeberry (*Rhamnus californica*) along with some California sagebrush (*Artemisia californica*) (Ecological Subregions of California, 2011). The coastal scrub community is usually a successional plant community that, in the absence of fire, gradually moves into herbaceous cover where the soil depth transitions from the shallowest to intermediate depth. The herbaceous plant community includes California annual grassland series and California Oat grass series. Coastal sage scrub and chaparral are known as secondary pioneer plant in California grasslands, which invade grassland and increase in the absence of fire or grazing. We noted a propagation of the introduced Cape ivy (*Delairea odorata*) during our field work. Cape ivy, a vine native to South Africa, has become a significant threat to coastal scrub.

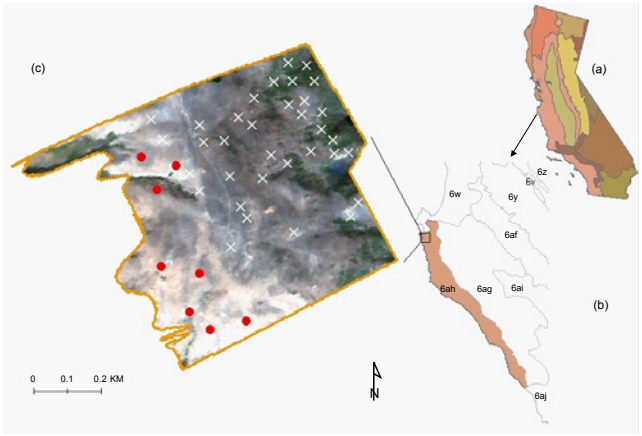

Figure 1: Study Area with (a) US Level III Ecoregions in California [49] (b) US Level IV Ecoregions: 6ah *Santa Lucia Coastal Forest and Woodland*, (c) True color AVIRIS imagery of the Brazil Ranch study site (central wavelengths: 638nm, 550nm, and 462nm). The white cross symbols are locations of field sample plots and the red circles represent plots selected using IKONOS imagery

	Acquired date	Parmeters
AVIRIS	September 24, 2008	224Bands, 3.5 m
PALSAR	April 14, 2008	FBS, HH, 6.25m
	July 18, 2008	FBD, HV, 12.5m
Landsat TM	May 13, 2008	(P043/R035) 30m
	September 18, 2008	(P043/R035) 30m
IKONOS	March 08, 2007	4m

Table 1: Remote sensing imagery used in this study.

Remote Sensing Datasets

Hyperspectral AVIRIS imagery provided information related to the biochemical state of the herbaceous-coastal scrub ecotype. AVIRIS collects data in 224 continuous channels of approximately 10-nanometer band pass over the spectral-wavelength range of 0.35-2.50 μm (from visible light to Near-infrared). A nominal pixel size of 3.5 m was collected by NASA/JPL on September 24, 2008, at approximately 9:40 a.m. local time. The AVIRIS imagery was Ortho-corrected by NASA/JPL using a full three-dimensional ray tracing method [16]. Each pixel in the image was individually ray traced using the best-estimate of sensor location and attitude until it intersected the DEM. The spatial fidelity of the data was much improved from previous datasets, especially in areas of rugged and variable across-track terrain, resulting in an accuracy of one pixel.

The AVIRIS imagery was captured mainly for the purpose of assessing the burn severity of Big Sur wildfires that occurred in 2008 (but which did not spread into the Brazil Ranch property; Table 1). Landsat 5 Thematic Mapper (TM) data were used to generate boundaries of the 2008 Big Sur wildfires and to clip the burnt area from the AVIRIS data set. Two cloud-free TM scenes (Path 43, Row 35) were selected from May 13, 2008 (pre-fire) and September 18, 2008 (post-fire).

An IKONOS image (acquired on March 08, 2007) was used to visually select 8 vegetation plots, since cliffs and steep slopes at the site made these areas otherwise inaccessible for *in-situ* survey assessment. Brovey transform (resolution merge) was applied on the selected IKONOS image to merge multispectral and panchromatic bands [17], and improve the spatial resolution to nearly 1 meter in the VIS/NIR bands.

PALSAR measurements were analyzed for sensitivity to the surface geometry and the dielectric constant of the illuminated surface. ALOS was launched in January 2006 by Japan Aerospace Exploration Agency (JAXA), which offered a Quad-polarization operation mode. We acquired PALSAR data over the research area for April 14, 2008 with a Fine Beam Single polarization (FBS, look angle 34.3°, HH-polarization, and a 6.25 m × 6.25 m ground resolution) and for July 18, 2008 with Fine Beam Double Polarization (FBD, look angle 34.3°, HV-polarization, ground resolution approximately 12.5 m × 12.5 m). In FBS mode, ALOS/PALSAR was operated in HH-polarization with a bandwidth of 28 MHz. In FBD mode, the polarization option was HH/HV at 14-MHz bandwidth. The operating sensor frequency is 1.27 GHz, which corresponds to a wavelength of 23.6 cm (L-band).

We acquired PALSAR data from one of the ALOS data nodes at the Alaska Satellite Facility (ASF). The SAR dataset was preprocessed to a 1.5 product level. The ASF performed the following steps: range compression using Fast Fourier Transform (FFT), secondary range compression using range migration compensation, range migration curvature corrections, azimuth compression, multi-look processing, and conversion from slant to ground range [18].

Methods

Field survey methods

From September through December of 2010, we inventoried 43 vegetation plots within Brazil Ranch, including 8 plots that were visually selected for high bare ground cover from the 1-m IKONOS imagery (due to steep slopes that made the survey plots otherwise

inaccessible) [19]. We established circular plots area with a radius of 17 m. Plots were set up by marking a center point and estimating vegetation percentage within a 17 m radius around the center point. Each plot was divided into four quads to improve the precision. Four field-crew members each independently estimated vegetation fraction percentages (herbaceous, coastal scrub and bare ground) in each quad by ocular estimation. Ocular estimation is an accurate and widely employed method for vegetation evaluation [11,20-22]. We compiled and averaged four quads to arrive at final vegetation cover estimation for each plot. The center location of each plot was positioned by Garmin GPSMAP 60CX unit in carrier phase (set to maximize spatial accuracy). The coordinates of plot center were differentially corrected by the National Geodetic Survey using the network of base station data (NGS, http://www.ngs.noaa.gov/CORS/Data.html).

Wildfire boundaries from TM imagery

We used a remotely sensed burn severity index called Differenced Normalized Burn Ratio (dNBR) derived from TM data to delineate the 2008 wildfire boundary. The TM sensor is appropriate for burn severity analysis because it records Near Infrared (NIR) and Middle Infrared (MIR) reflectance in bands 4 and 7, respectively. TM4 is primarily dependent on the refractive index of leaf morphology and discontinuities within the leaf [23] while TM7 is sensitive to water content in both soils and vegetation [24].

The TM images were converted into radiance and then at-sensor reflectance using instrument gains and offsets. The MODTRAN4 model was further used for atmosphere correction [25]. The spectral index of NBR was calculated from TM4 and TM7 (with central wavelength of 0.83 and 2.22 μm, respectively) bands according to [Eq. (1)] [26,27].

$$NBR = (NIR - MIR) / (NIR + MIR) \quad (1)$$

dNBR is the multi-temporal difference of pre- and post-fire NBR [28], defined as:

$$dNBR = NBR_{prefire} - NBR_{postfire} \quad (2)$$

Hyperspectral image processing

The AVIRIS dataset was clipped to the 2008 dNBR fire boundary. We converted AVIRIS radiance to reflectance via atmospheric correction using the FLAASH algorithm. The FLAASH method is based on observations by Kaufman [29], of a nearly fixed ratio between the reflectances of pixels at 660 nm and 2100 nm. It performs a second and final MODTRAN4 calculation loop over water.

Atmospherically corrected AVIRIS data were used to calculate vegetation indices. Four indices (NDVI, OSAVI, TCARI, and PRI) were selected in this study to generate spectral space for extraction of vegetation information [Eq. (3),(4),(5),(6)). These indices have been related to Leaf Area Index (LAI) and vegetation biochemical state, including chlorophyll absorption or other specific features.

The Normalized Difference Vegetation Index (NDVI) is a measure of vegetation greenness cover [30,31], and can be used to discriminate vegetated from bare ground. AVIRIS Optimized Soil Adjusted Vegetation Index (OSAVI) represented improvements in the dynamic range or decreased sensitivity to differences in soil backgrounds [32]. The chief advantages of OSAVI are its simplified formulation and the lack of a requirement for *a priori* knowledge of the soil type. This index is suitable for vegetation applications since the residual variation in OSAVI is evenly spread across the full range of vegetation index response.

AVIRIS Transformed Chlorophyll Absorption in Reflectance Index (TCARI) provides information to estimate the active radiation absorbed for photosynthesis. The combination of TCARI/OSAVI permits a qualitative estimation of the chlorophyll content of leaves [33]. AVIRIS Photochemical Reflectance Index (PRI) measures xanthophyll activity, which is usually applied to vegetation detection prior to senescence [34].

$$NDVI = (R_{831} - R_{638}) / (R_{831} + R_{638}) \quad (3)$$

$$OSAVI = (1+ 0.16) \times (R_{800} - R_{670}) / (R_{800} + R_{670} + 0.16) \quad (4)$$

$$TCARI= 3 \times [(R_{700} - R_{670}) - 0.2 \times (R_{700} - R_{550}) \times (R_{700} / R_{670})] \quad (5)$$

$$PRI = (R_{531} - R_{570}) / (R_{531} + R_{570}) \quad (6)$$

PALSAR processing

Radiometric calibration: Radiometric calibration of PALSAR data was carried out using the following method [Eq. (7)]. Digital numbers (the amplitude of the backscattered signal) of PALSAR data were transformed into a backscattering coefficient (in decibels).

$$\sigma_i^{\circ}(dB) = 20 * \log_{10}(DN_i) + Kdb \quad (7) \quad [18]$$

Where the calibration constant for PALSAR L1.5 products is Kdb = -83 dB.

Radiometric terrain correction: Radar backscatter is significantly impacted by terrain undulations. Slope-induced distortions can have a direct impact on radiometric quality [6,35,36]. The correction of these effects becomes important when quantitative image analysis is performed with respect to geo- and biophysical parameters [37]. A 10-m resolution Digital Elevation Model (DEM) was used to correct terrain induced distortions (United States Geological Survey (USGS), National Elevation Dataset (NED)). Based on a lookup table describing the transformation between the radar and map geometry, Ulander [38] developed an approach [Eq. (8) and (9)] to minimize the dependence on terrain undulation [37]. The lookup table was generated using the NED DEM and the orbital information of the PALSAR data. The normalized, terrain-corrected radar backscattering coefficient is defined as:

$$\sigma^0_{Correct} = \bar{\beta} \cos\psi = \frac{\sigma^0}{\sin\theta_{loc}} \cos\psi \quad (8)$$

where is $\bar{\beta}$ the averaged radar brightness and ψ is the projection angle between the surface normal and the image plane normal, which varies between 0°and 90°, and θ_{loc} is the local incidence angle. We note that ψ is the complementary angle to the smallest angle between the surface normal and the image plane.

Calculation of $\cos\psi$ is given by Eq. (9)

$$\cos(\psi) = \sin(\theta).\cos(u) + \cos(\theta).\sin(u).\sin(v) \quad (9)$$

Where θ is the local incidence angle of a horizontal surface patch (i.e. ellipsoidal incidence angle), and u, v are terrain slope and aspect of the surface relative the vertical and azimuth directions, which are calculated from the DEM [38].

We note that, in the correction for slope-induced backscattering distortion, the backscattering coefficient tends to vary (decrease) with increasing local incidence angle (θ) in the non-radiometric corrected (but terrain-corrected) curve, while the radiometric-corrected data

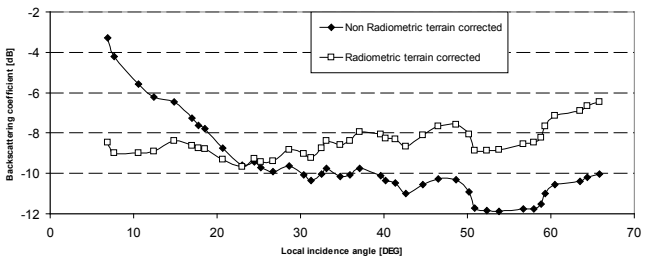

Figure 2: SAR backscattering coefficient as a function of local incidence angle before and after geometric and radiometric terrain correction.

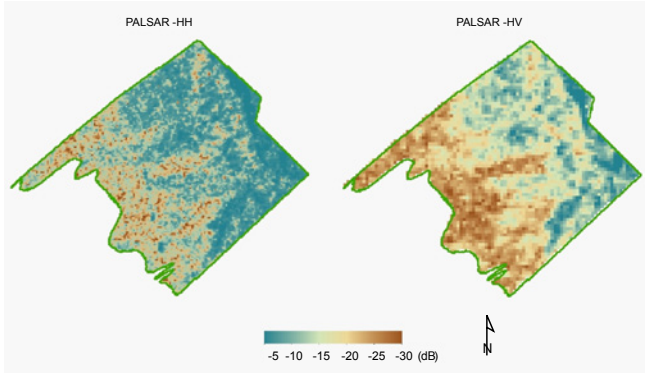

Figure 3: Radiometric corrected PALSAR data with backscatter coefficient in dB.

shows a stable backscattering coefficient over the local incidence angle (Figure 2).

Radiometric corrected PALSAR backscattering coefficients (HH and HV) were co-registered with the AVIRIS imagery and resampled at the same spatial resolution as AVIRIS (Figure 3). Co-registration accuracy was estimated to be 0.5 pixels. The speckle noise in PALSAR backscattering coefficients was minimized by applying Lee-Sigma filters with a 5 × 5 moving-window before textural information extraction [39].

Textural feature extraction from PALSAR data: Three texture features called energy, contrast, homogeneity were extracted from PALSAR backscattering coefficients by using the method of co-occurrence matrices (GLCM). The fractal dimension of PALSAR backscattering coefficients was extracted using the triangular prism surface area method (TPSAM) [40]. These four features were generated from HH- and HV-polarizations comprising a set of 2 × 4 bands.

Energy is also called the angular second moment [41], which measures textural uniformity. Contrast is the spatial frequency that represents the amount of the local variation in the scene. Local homogeneity is called the inverse difference moment. For a specific vegetation area, local homogeneity and contrast are inversely correlated, while energy is kept constant. On the other hand, local homogeneity and energy are inversely correlated, while contrast remains constant. Fractals measure the roughness attributes in the SAR data.

Classification scheme

Endmember selection: Image pixels within the Brazil Ranch study area were visually separated into two types based on their land cover composition: pure pixels covered entirely by a single cover class (herbaceous, coastal scrub, or bare ground), and mixed pixels composed of combinations of the above-mentioned classes. Three endmembers were identified from the pure pixels and classified by using a priori information from a spectral library [24].

The following steps were performed to reach aforementioned outcome: First, we used rotation transforms on AVIRIS imagery. Minimum Noise Fraction Transform (MNF) is an algorithm designed to determine the inherent dimensionality of hyperspectral imagery, segregate noise in the data, and reduce the computational requirements for subsequent processing [42]. A threshold value of 0.27 was selected based on the plots of spatial coherence and eigenvalues. This threshold identified the first 39 bands in MNF space to be used for spectral information extraction, while the remaining bands were considered noise.

Next, we used the Pixel Purity Index (PPI) [43] to find the most spectrally pure pixels in the MNF space. The PPI was computed by repeatedly projecting n-D scatter plots onto a random unit vector. Each resulting value corresponded to the number of times that a pixel was recorded as extreme. A threshold value of 20 was selected as critical value for space partitioning in our study area.

Lastly, the pure pixels were separated into three classes. The spectral library provided by Elvidge [24] was selected as a priori information to perform supervised Bayes Maximum Likelihood classification [44]. The Elvidge spectral library was measured as hemispherical reflectance using a Beckman UV-5240 spectrophotometer at Jasper Ridge in central California, which included all the vegetation species (in both dry and wet seasons) also found in the Brazil Ranch study site. Each pure pixel was categorized as one of the three classes, namely, herbaceous, coastal scrub, and bare ground (Figure 4).

Construction of the new feature space: Pixels with a PPI value less than 20 were identified and a new 3-D feature space was constructed to combine spectra information, index features, and L-band textural information for fractional decomposition. The new feature space was composed of 50 bands (39 bands generated by MNF from AVIRIS imagery, 3 bands from AVIRIS vegetation indices, and 2×4 texture bands from PALSAR data).

For the first dimension, basic spectral information was provided by the 39 MNF bands. Examination of the vegetation and soil information contained in the MNF-transformed data, together with the associated eigenvalues, indicated that 94% of the total statistical variance in the AVIRIS imagery was contained in the first 39 MNF bands of the image. For the second dimension, phenological characteristics of vegetation were observed in all three indices. Annual herbaceous species dominate

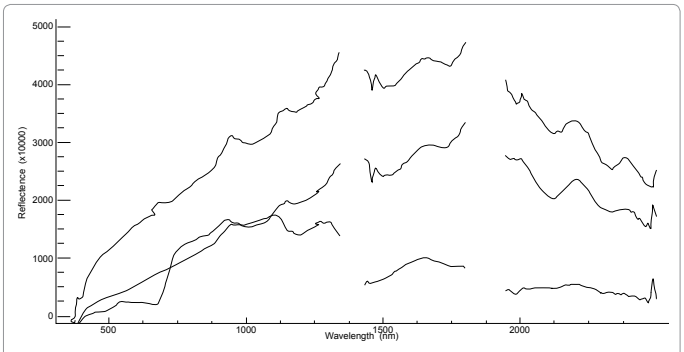

Figure 4: Spectral endmembers derived from AVIRIS data, constrained by the PPI threshold and identified by the spectral library from Elvidge [22].

the great majority of the grasslands in Big Sur. Most of the herbaceous materials had senesced, and coastal scrub was still green or light-green when our AVIRIS data was acquired. Peak green season in the central coast region of California occurs from around February 15 to March 20, after which herbaceous vegetation cover gradually turns brown. TCARI/OSAVI and PRI provided the needed information for phenological vegetation discrimination. The ratio of TCARI/OSAVI is especially useful when herbaceous vegetation, coastal scrub, and bare ground were co-located in a pixel. For the third dimension, the 2 × 4 texture features from SAR data were used [45, 46].

Decomposition from OLS: OLS regression is widely used to infer linear regression model parameters in the remote sensing literature [47]. We applied OLS regression on the 3-D feature space constructed from 50 bands. Signatures of the pure pixels (assigned 100% coverage of either herbaceous, coastal scrub, or bare ground) were used as explanatory variables in the OLS regression with each mixed pixel's spectral signature as the response variable.

The generalized decomposition model is described as Eq. (10):

$$\hat{R} = \beta_0 + \beta_{HBV} R_{HBV} + \beta_{CSS} R_{CSS} + \beta_{BG} R_{BG} + \varepsilon \quad (10)$$

where $\hat{R}$ is the modeled mixed pixel feature vector in the new combined feature space, β_n s are coefficients, R_n s refer to herbaceous vegetation, coastal scrub, and bare ground respectively, and ε is random error term.

Three continuous raster layers were generated by OLS analysis as the proportion of each cover type represented in the mixed pixels. A composite fractional coverage map was generated from the three mixed raster layers merged with the pure pixels. This overall approach is summarized in a general flow chart (Figure 5).

Results

Fractional vegetation mapping

The mean value of herbaceous cover was higher at Brazil Ranch than the other two cover types at around 51.6%, and was generally highest on the south-facing ridge top locations. The percentage of herbaceous cover declined gradually with decreasing elevation toward the northeast (Figure 6). Coastal scrub was distributed more across the valley and the gently sloping areas. The mean cover value for coastal scrub at the site was 21.9%. Bare ground often coexisted with herbaceous cover on ridge tops, but we also detected scattered patches of coastal scrub on the steep slopes.

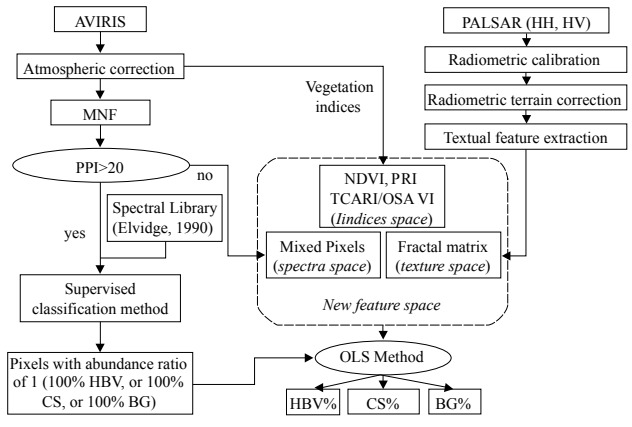

Figure 5: General flow charts of the fractional vegetation cover mapping. Solid lines represent AVIRIS and PALSAR processing steps separately, while the dashed line includes the fusion of these two processing steps in the new feature space.

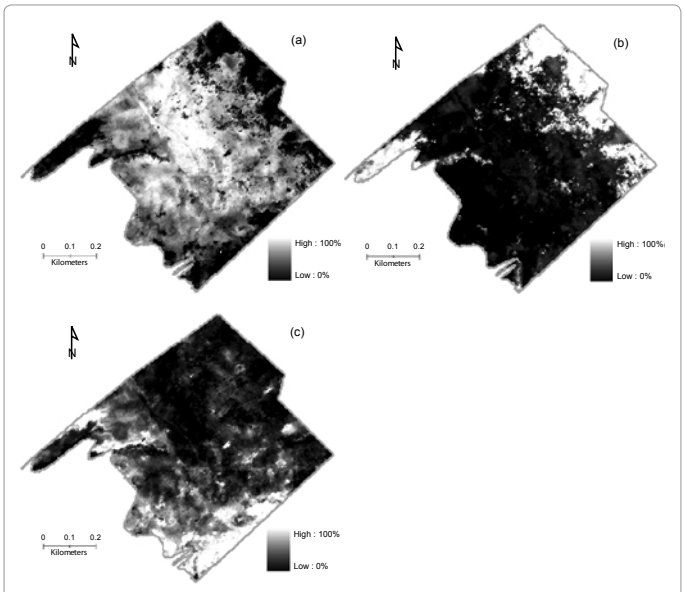

Figure 6: Fractional vegetation cover mapping: (a) herbaceous, (b) coastal scrub, (c) bare ground.

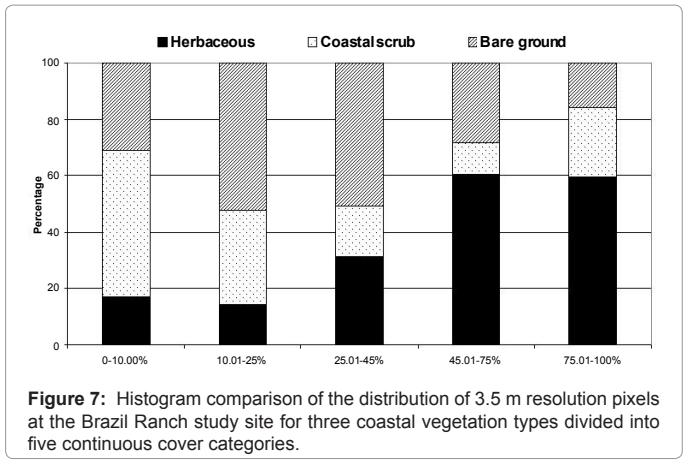

Figure 7: Histogram comparison of the distribution of 3.5 m resolution pixels at the Brazil Ranch study site for three coastal vegetation types divided into five continuous cover categories.

In order to evaluate the landscape patterns more readily, the three maps (Figure 6) were reclassed into five continuous categories of fractional cover at the 3.5 m resolution: less than 10%, 10.01-25.00%, 25.01-45.00%, 45.01-75.00%, and more than 75.01%. A histogram comparison of the three cover types (Figure 7) showed that, for the pixels having a coverage fraction of 45% or greater of any single cover type, herbaceous vegetation predominated in those areas. For the pixels having a coverage fraction of 10% or less of any single cover type, coastal scrub predominated in those areas. For the pixels having a coverage fraction between 10% and 45% of any single cover type, bare ground predominated.

An Iso-clustering algorithm [44,48] was further used to characterize the landscape pattern. Five ecotypes were determined by the combination of different cover percentages (Figure 8). The first three ecotypes were dominated by the individual coverages of herbaceous, coastal scrub, and bare ground with percentage of 86%, 89%, and 77%

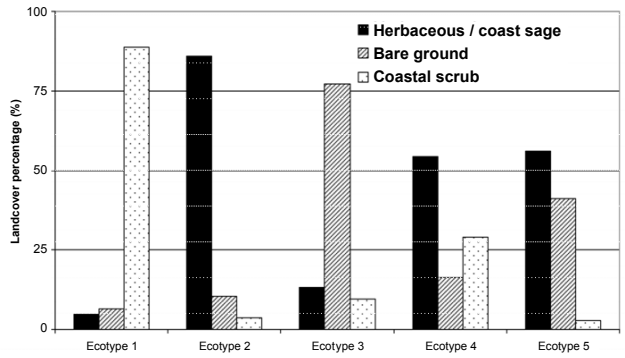

Figure 8: Composition of Big Sur coastal vegetation ecotypes by fractional coverage.

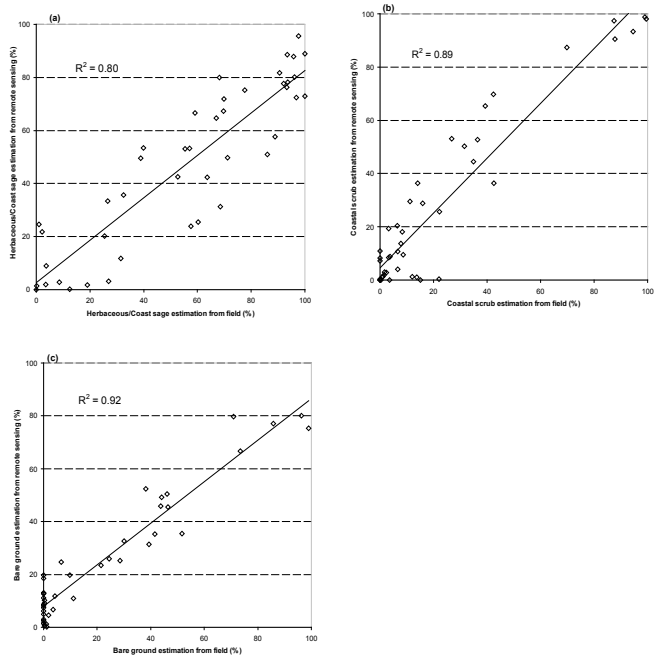

Figure 9: Comparison of (a) herbaceous, (b) coastal scrub, and (c) bare ground fractional coverages between field survey estimation and remote sensing predictions.

respectively. The fourth mixed ecotype was composed of coastal scrub (more than 50%), herbaceous (around 30%), and bare ground (less than 20%). The fifth ecotype was dominated by a combination of coastal scrub (56%) and bare ground (41%).

Fractional coverage accuracy assessment

We compared field survey estimations of vegetation fractional cover to remote sensing predictions from a fusion of SAR and hyperspectral imagery (Figure 9). Linear regression results produced coefficients of determination for herbaceous, coastal scrub, and bare ground cover of R^2 = 0.80, 0.89, and 0.92, respectively. The estimated accuracy of fractional coverage mapping from remote sensing was calculated in terms of Root Mean Square Error (RMSE) at 17%, 12%, and 10% for herbaceous, coastal scrub, and bare ground, respectively.

Contributions assessment

We examined the relative contributions of vegetation index features and textural information to the combined OLS analysis results (Table

-	HB_*Indices*	CS_*Indices*	BG_*Indices*	HB_*E*	CS_*E*	BG_*E*
HB_*Indices*	1.00					
CS_*Indices*	-0.65	1.00				
BG_*Indices*	-0.70	-0.09	1.00			
HB_*E*	0.75	-0.45	-0.56	1.00		
CS_*E*	-0.33	0.75	-0.28	-0.56	1.00	
BG_*E*	-0.49	-0.27	0.90	-0.54	-0.40	1.000

Abbrreviations: HB_*Indices*, CS_*Indices*, and BG_*Indices* represent percentage value derived from the feature space directly, whereas HB_*E*, CS_*E*, and BS_*E* represent the final combined percentage values for herbaceous (HB), coastal scrub (CS), and bare ground (BG) coverages

Table 2: Pearson correlation (*R*-values) of the percentage derived from AVIRIS indices feature space and the combined feature space of the OLS results.

-	HB_*Texture*	CS_*Texture*	BG_*Texture*	HB_*E*	CS_*E*	BG_*E*
HB_*Texture*	1.00					
CS_*Texture*	-0.52	1.00				
BG_*Texture*	N/A	N/A	1.00			
HB_*E*	0.09	0.19	N/A	1.00		
CS_*E*	0.30	0.62	N/A	-0.56	1.00	
BG_*E*	-0.21	-0.09	N/A	-0.54	-0.40	1.00

Abbrreviations: HB_ *Texture*, CS_*Texture*, and BG_*Texture* represent percentage value derived from the feature space directly, whereas HB_*E*, CS_*E*, and BS_*E* represent the final combined percentage values for herbaceous (HB), coastal scrub (CS), and bare ground (BG) coverages.

Table 3: Pearson correlation (R-values) of the percentage derived from PALSAR texture feature space and the combined feature space of the OLS results.

2 and Table 3). First, relationships of separate features to measured percent cover data sets were determined by simple regression. These outcomes were then compared to the predictions of percent cover from the combined feature space (labeled as E contributions). A higher R value indicates higher contribution from indices space to the combined feature space, as shown in the rows of Tables 2 and 3 as *E* contributions.

Features in each of the vegetation indices contributed to discrimination of bare ground to a higher degree than for the other two vegetation classes, while textural information contributed to the discrimination of coastal scrub to a higher degree than for the other two classes. The index features were directly related to the photosynthetic capacity and, hence, the energy absorption of vegetation. This association contributed notably to the discrimination of herbaceous cover from the soil background. For example, PRI index values would be low and declining during the growth phase of the grass canopy and increase rapidly during the senescence period, whereas the PRI would remain relatively constant year-round for bare ground areas.

L-band SAR data contributed useful information to detecting the coverage of coastal scrub (Table 3), with an R valus of 0.62, but made no contribution to the detection of bare ground. The L-band SAR (wavelength ~24 cm) has the advantage of obtaining better coherence than C-band SAR in dense vegetation. This advantage is due to the L-band's capacity to penetrate the coastal scrub canopy and scatter off trunks and branches, thereby distinguishing woody tissues of shrubs from herbaceous cover.

We summarized the results using OLS methods to decompose the fractional vegetation coverages from the combined feature space using the inputs of HV, HH, NDVI, PRI and TCARI/OSAVI in Table 4. Variance Inflation Factor (VIF) values were lower than 7.5 for all input variables (except for that of TCARI/OSAVI) which indicated no explanatory variable redundancy during the weighted decomposition

a. Coastal scrub cover							
	Variable	Coefficient	t-Statistic	Probability	Robust t	Robust Pr	VIF
	Intercept	-67.77	-3.11	0.0025 **	-4.276	0.0001 **	
	HV	-1.027	-0.95	0.34	-0.81	0.418	5.28
	HH	1.627	1.488	0.140	1.361	0.177	5.15
	NDVI	171.34	9.68	0.000 **	10.171	0.000 **	3.01
	PRI	-4.5E-05	-1.56	0.122	-1.588	0.116	4.41
	TCA_OSA	0.00008	0.014	0.989	0.014	0.989	7.19
b. Herbaceous cover							
	Variable	Coefficient	t-Statistic	Probability	Robust t	Robust Pr	VIF
	Intercept	158.20	3.63	0.0005 **	3.375	0.001 **	
	HV	4.173	1.94	0.06 *	1.76	0.082 *	5.28
	HH	-4.287	-1.96	0.053 *	-2.285	0.025 **	5.15
	NDVI	-152.72	-4.31	0.00005 **	-3.33	0.001 **	3.01
	PRI	0.00028	4.83	0.00001 **	2.870	0.005 **	4.42
	TCA_OSA	0.0043	0.382	0.703	0.312	0.755	7.19
c. Bare ground cover							
	Variable	Coefficient	t-Statistic	Probability	Robust t	Robust Pr	VIF
	Intercept	9.57	0.26	0.79	0.235	0.815	
	HV	-3.147	-1.74	0.08 *	1.65	0.102	5.28
	HH	2.66	1.45	0.15	1.794	0.076 *	5.15
	NDVI	-18.62	-0.63	0.53	0.47	0.649	3.01
	PRI	-0.00023	-4.83	0.00001 **	2.747	0.007 **	4.41
	TCA_OSA	-0.0044	-0.465	0.64	-0.380	0.705	7.19

* Statistically significant at the 0.1 level and ** at the 0.05 level
Robust t-test and Pr (probability) are the values under an assumption of non-normally distributed data.
Large VIF (> 7.5, for example) indicates explanatory

Table 4: Summary of explanatory variable OLS results for vegetation cover classes at Brazil Ranch.

[49]. VIF quantifies the degree of multicollinearity in an OLS regression analysis. It provides a measure of how much the variance of an estimated regression coefficient (the square of the estimate's standard deviation) is increased because of collinearity. Robust regression results were included in Table 3 to evaluate the effects of bad leverage outliers that would otherwise bias the parameter estimation with a non-normal distribution. A robust determination down-weights outliers and also accounts for non-normality in sample distributions. The results of these two parameters (t-test and Robust Probability) indicated that the SAR HV or HH explanatory variables were statistically significant ($p < 0.1$) in the OLS for herbaceous and bare ground covers.

Discussion

Remote sensing is the only practical method to map vegetation types in the steep and inaccessible mountains and valleys of the central Pacific coast. The results presented in our study offer a baseline mapping estimate of vegetation status in an area of the western United States subject to extreme weather events, climate change, and regular wildfires [27]. The methods described above can be replicated in years to come to assess even subtle changes in central California's coastal vegetation cover.

In ecosystems of the Central Coast, radar backscatter signals received from the terrestrial surface included many pixels with mixed vegetation cover. The backscatter coefficient is contingent on incident angle, wavelength, polarization, surface roughness, and dielectric properties of the surface. The three basic endmembers in our study area have backscattering coefficients that varied significantly. Specular or surface scattering occurred in the area dominated by herbaceous and bare ground. Volume scattering and double bounce scattering occurred in coastal scrub dominated areas. Volume and surface scattering played an important role in the response from coastal scrub plant communities, which increased the overall backscatter magnitude because of the presence of and interaction among different scattering mechanisms.

Our results showed that the fusion of hyperspectral imagery and L-band SAR data can be used for accurate fractional vegetation mapping in the herbaceous-shrub communities of coastal California. The most striking results were obtained with the addition of L-band SAR texture features to help discriminate herbaceous cover from coastal scrub. Textural information from SAR data improved the fractional decomposition significantly. Expanded map products for vegetation fractional cover can next be ingested into biogeochemical cycling models [50,51] for the entire central California coastal region to improve annual plant production and fuel biomass loading predictions.

Acknowledgements

This research was supported by an appointment of the first author to the NASA Postdoctoral Program at the NASA Ames Research Center, administered by Oak Ridge Associated Universities through a contract with NASA. The authors are grateful to the U. S. Forest Service, Los Padres National Forest (Ecosystem Manager Jeff Kwasny), for providing access to the Brazil Ranch property. The authors would like to thank NASA JPL for AVIRIS data acquisition and preprocessing in 2008.

References

1. Stow D, Hamada Y, Coulter L, Anguelova Z (2008) Monitoring shrubland habitat changes through object-based change identification with airborne multispectral imagery. Remote Sensing of Environment 112: 1051-1061.
2. Stow D, Coulter L, Johnson A, Petersen A (2004) Monitoring detailed land-cover changes in shrubland habitat reserves using multi-temporal IKONOS data. Geocarto International 19: 95-102.
3. Coulter L, Stow D, Baer S (2003) A frame center matching technique for precise registration of multitemporal airborne frame imagery: Methods and software approaches. IEEE Trans. Geosci Remote Sens 41: 2436-2444.
4. Riano D, Chuvieco E, Ustin S, Zomer R, Dennison P, et al. (2002) Assessment

of vegetation regeneration after fire through multitemporal analysis of AVIRIS images in the Santa Monica Mountains. Remote Sensing of Environment 79: 60-71.

5. Le Toan T, Beaudoin A, Riom J, Guyon D (1992) Relating forest biomass to SAR data. IEEE Trans. Geosci. Remote Sens 30: 403-411.
6. Musick HB, Schaber GS, Breed CS (1998) AIRSAR studies of woody shrub density in semiarid rangeland: Jornada del Muerto, New Mexico. Remote Sensing of Environment 66: 29-40.
7. Santoro M, Askne J, Smith G, Fransson E S (2002) Stem volume retrieval in boreal forests from ERS-1/2 interferometry. Remote Sensing of Environment 81: 19-35.
8. Engdahl ME, Pulliainen JT, Hallikainen MT (2004) Boreal forest coherence based measures of interferometric pair suitability for operational stem volume retrieval. IEEE Trans Geosci Remote Sens 1: 228-231.
9. Jouan A, Allard Y (2004) Land use mapping with evidential fusion of features extracted from polarimetric aperture radar and hyperspectral imagery. Information Fusion 5: 251-267.
10. Huang S, Crabtree RL, Potter CS, Gross P (2009) Estimating the quantity and quality of coarse woody debris in Yellowstone post-fire forest ecosystem from fusion of SAR and optical data. Remote Sensing of Environment 113: 1926-1938.
11. Huang S, Potter C, Crabtree R, Hager S, Gross P (2010) Fusing optical and radar data to estimate sagebrush, herbaceous, and bare ground cover in Yellowstone. Remote Sensing of Environment 114: 251-264.
12. Yatabe SM, Leckie DC (1996) Clearcut and forest-type discrimination in satellite SAR imagery. Canadian Journal of Remote Sensing 21: 455-467.
13. Clark ML, Roberts DA, Clark DB (2005) Hyperspectral discrimination of tropical rain forest tree species at leaf to crown scales. Remote Sensing of Environment 96: 375-398
14. Moghaddam M, Dungan J, Acker S (2002) Forest variable estimation from fusion of SAR and multispectral optical data. IEEE Trans. Geosci Remote Sensing 40: 2176-2187.
15. Blaschke T, Lang S, Hay GJ (2008) Object-based image analysis: spatial concepts for knowledge-driven remote sensing applications. Verlag Gmbh Springer : 493-512.
16. Schläpfer D, Hausold A, Richter R (2000) A Unified Approach to Parametric Geocoding and Atmospheric/Topographic Correction for Wide FOV Airborne Imagery Part 1: Parametric Ortho-Rectification Process. Proc. 2nd EARSeL Workshop on Imaging Spectroscopy, EARSeL, Enschede: 9.
17. Pohl C, Van Genderen JL (1998) Multisensor image fusion in remote sensing: concepts, methods and application. Int J Remote Sens 19: 823-854.
18. ALOS products (2007) Information ALOS PALSAR products for ADEN users. Reference: ALOS-GSEG-EOPG-TN-07-0001, ESA.
19. Zhou G, Li R (200) Accuracy evaluation of ground points from IKONOS high resolution satellite imagery. Photogrammetric Engineering and Remote Sensing 66: 1103-1112.
20. Hatton TJ, West NE, Johnson PS (1986) Relationships of the error associated with ocular estimation and actual total cover. Journal of Range Management 39: 91-92.
21. Bråkenhielm S, Liu Q (1995) Comparison of field methods in vegetation monitoring. Water, Air, and Soil Pollution 79: 75-87.
22. Symstad AJ, Wienk CL, Thorstenson AD (2008) Precision, repeatability, and efficiency of two canopy-cover estimate methods in Northern Great Plains vegetation. Rangeland Ecology and Management 61: 419-429.
23. Puritch GS (1981) Nonvisual remote sensing of trees affected by stress: A review. Vicotri Canadian Forestry Service Forestry Technical Report BC-X-30, Pacific Forestry Centre.
24. Elvidge CD (1990) Visible and infrared reflectance characteristics of dry plant materials. Int J Remote Sens 11: 1775-1795.
25. Adler-Golden SM, Matthew MW, Bernstein LS, Levine RY, Berk A, et al. (1999) Atmospheric Correction for Short-wave Spectral Imagery Based on MODTRAN4.
26. De Santis A, Asner GP, Vaughan PJ, Knapp DE (2010) Mapping burn severity and burning efficiency in California using simulation models and Landsat imagery. Remote Sensing of Environment 114: 1535-1545.
27. Lopez-Garcia M, Caselles V (1991) Mapping burns and natural reforestation using Thematic Mapper data. Geocarto International 6: 31-37.
28. Key C, Benson N (2005) Landscape assessment: Ground measure of severity; the Composite Burn Index, and remote sensing of severity, the Normalized Burn Index. In D. Lutes, R. Keane, J. Caratti, C. Key, N. Benson, S. Sutherland, and L. Gangi (Eds.), FIREMON: Fire effects monitoring and inventory system General Technical Report RMRS-GTR-164-CD LA Rocky Mountains Research Station: USDA Forest Service: 1-51.
29. Kaufman YJ, Wald AE, Remer LA, Gao BC, Li RR, et al. (1997) The MODIS 2.1-μm Channel-Correlation with Visible Reflectance for Use in Remote Sensing of Aerosol. IEEE Trans Geosci Remote Sens 35: 1286-1298.
30. Rouse JW, Haas RH, Schell JA, Deering DW, Harlan JC (1974) Monitoring the vernal advancements and retrogradation of natural vegetation. Remote Sensing Center 371.
31. Bannari A, Morin D, Bonn F, Huete A (1995) A review of vegetation indices. Remote Sensing Reviews 13: 95-120.
32. Rondeaux G, Steven M, Baret F (1996) Optimization of soil-adjusted vegetation indices. Remote Sensing of Environment 55: 95-107.
33. Haboudane D, Miller J, Tremblay N, Zarco-Tejada P (2001) Combining hyperspectral vegetation indices for a better estimation of leaf chlorophyll content in corn canopies. In: Proc. International Symposium on Spectral Sensing Research (ISSSR), Quebec City (Canada), June 10th-15th.
34. Gamon JA, Peñuelas J, Field CB (1992) A narrow-waveband spectral index that tracks diurnal changes in photosynthetic efficiency. Remote Sensing of Environment 41: 35-44.
35. MGelautz M, Frick H, Raggam J, Burgstaller J, Leberl F (1998) SAR image simulation and analysis of alpine terrain. ISPRS Journal of Photogrammetry and Remote Sensing 53: 17-38.
36. Goyal SK, Seyfried MS, O'Neill PE (1999) Correction of surface roughness and topographic effects on airborne SAR in mountainous rangeland areas. Remote Sensing of Environment 67: 124-136.
37. Loew A, Mauser W (2007) Generation of geometrically and radiometrically terrain corrected SAR image products. Remote Sensing of Environment 106: 337-349.
38. Longnecker M T, Ott R L (2004) A First Course in Statistical Methods. Cole: Thomson Brooks.s: 615.
39. Ulander L (1996) Radiometric slope correction of synthetic-aperture radar images. IEEE Trans Geosci Remote Sens 34: 1115-1122.
40. Lee J (1981) Speckle analysis and smoothing of synthetic aperture radar images. Comput Graph Image Process 17: 24-32.
41. Pant T, Singh D, Srivastava T (2010) Advanced fractal approach for unsupervised classification of SAR images. Advances in Space Research 45: 1338-1349.
42. Haralick M, Shanmugam K, Dinstein I (1973) Textural features for image classification. IEEE Trans on Systems Man Cybernet 3: 610-621.
43. Green AA, Berman M, Switzer P, Graig MD (1988) A transformation for ordering multispectral data in terms of image quality with implications for noise removal. IEEE Trans Geosci Remote Sens 26: 65-74.
44. Boardman JW, Kruse FA, Green RO (1995) Mapping target signatures via partial unmixing of AVIRIS data. In Fifth JPL Airborne Earth Science Workshop 95: 23-26.
45. Asner GP, Heidebrecht KB (2003) Imaging spectroscopy for desertification studies: comparing AVIRIS and EO-1 Hyperion in Argentina drylands. IEEE Trans Geosci Remote Sens 41: 1283-1296.
46. Asner GP, Heidebrecht KB (2002) Spectral unmixing of vegetation, soil and dry carbon cover in arid regions: comparing multispectral and hyperspectral observations. Int J Remote Sens 23: 3939-3958.
47. Fernandes R, Leblanc SG (2005) Parametric (modified least squares) and non-parametric (Theil-Sen) linear regressions for predicting biophysical parameters

in the presence of measurement errors. Remote Sensing of Environment 95: 303-316.

48. Richards JA (1986) Remote Sensing Digital Image Analysis: An Introduction. Berlin: Springer-Verlag.

49. Ball GH, Hall DJ (1965) ISODATA, A Novel Method of Data Analysis and Pattern Classification. Menlo Park. California: Stanford Research Institute.

50. Potter C., Klooster S, Huete A, Genovese V (2007) Terrestrial carbon sinks for the United States predicted from MODIS satellite data and ecosystem modeling. Earth Interactions 11: 1-21.

51. Scott R Miles, Charles B Goudey, Earl B Alexander, John O Sawyer (1998) Ecological subregions of California : section & subsection descriptions. (R5-EM-TP-005-NET), San Francisco.